




# Quantum simulation of extended electron-phonon-coupling models in a hybrid Rydberg atom setup

João P. Mendonça \* and Krzysztof Jachymski 

*Faculty of Physics, University of Warsaw, Pasteura 5, 02-093 Warsaw, Poland*

 (Received 24 August 2022; revised 9 January 2023; accepted 28 February 2023; published 10 March 2023)

State-of-the-art experiments using Rydberg atoms can now operate with large numbers of trapped particles with tunable geometry and long coherence time. We propose a way to utilize this in a hybrid setup involving neutral ground-state atoms to efficiently simulate condensed-matter models featuring electron-phonon coupling. Such implementation should allow for controlling the coupling strength and range as well as the band structure of both the phonons and atoms, paving the way towards studying both static and dynamic properties of extended Hubbard-Holstein models.

DOI: [10.1103/PhysRevA.107.032808](https://doi.org/10.1103/PhysRevA.107.032808)

## I. INTRODUCTION

The quest for theoretical understanding of strongly correlated many-body systems is known to be extremely challenging. Classical simulation methods can become inefficient as the Hilbert space becomes too large to effectively sample. The number of parameters needed to describe and store a quantum state grows exponentially with the system size. Quantum computers hold the promise to overcome this difficulty, but near-term devices cannot be expected to provide the needed number of logical qubits and sufficient circuit depth. For these reasons, analog quantum simulators are among the most promising tools to study ground-state properties as well as dynamics of interacting quantum systems [1–3]. As the approach of analog simulation is to construct a controllable system that can reproduce the physics of a different one, it is nonuniversal and thus the details of experimental implementation matter. The platforms for quantum simulation must feature some versatility in tuning the system parameters, scalability in the number of qubits, and reliable measurement schemes. Over the past two decades, a wide range of promising quantum devices that may have some of the desired properties has emerged [4]. Among the various platforms available, ultracold neutral atoms [5] and Rydberg atom arrays [6] received a lot of attention in this respect. A hybrid approach involving a combination of setups can be promising as well, allowing for easier implementation of more complex systems with potentially independently tunable properties [7].

Strongly correlated materials can feature a competition between electron-electron and electron-phonon interactions which drive the system towards different ordered phases. Phonon-mediated attraction between electrons can enhance fermion pairing even when the Coulomb repulsion is strong [8,9]. In such materials, as well as high- $T_c$  superconductors, the Hamiltonians cannot generally be treated by perturbative methods because of the lack of a small parameter.

Computational methods such as exact diagonalization, quantum Monte Carlo, and density-matrix renormalization group greatly advanced the understanding of many-body systems. However, as the phonon Hilbert space has to be truncated, numerical studies typically allow only a small phonon number and system size.

A number of theoretical proposals for quantum simulation of electron-phonon models using molecules as well as ions exist [10–13]. However, they have stringent requirements and can lack versatility. For example, in order to crystallize the molecules one needs extremely low temperatures, while in ion-atom systems the relevant energy scales are quite separated. Here we focus on a different type of mixture involving an array of Rydberg atoms and a ground-state gas. In most experimental realizations, the Rydberg states are repelled by optical traps and the laser field must be turned off during experiments. However, recent developments allow for keeping the tweezer array on as well as achieving state-insensitive traps [14,15], leading to long lifetimes and opening the door towards a new simulation platform.

In this paper, we extend this notion and provide a scheme for quantum simulation of strongly correlated many-body systems. To begin, we study the phonon spectrum of a Rydberg chain, showcasing its tunability. Then we argue that the array can be seen as a periodic potential for the neutral atoms [see Fig. 1(a)]. Following that, we derive and study the full system Hamiltonian which contains atom-phonon coupling. Finally, we discuss further prospects for quantum simulation in this setup.

The simplest and widely used Hamiltonian that takes into account both electron-electron and electron-phonon interactions is the Hubbard-Holstein model:

$$\begin{aligned}
 H = & -t \sum_{\langle i,j \rangle \sigma} (c_{i\sigma}^\dagger c_{j\sigma} + \text{H.c.}) + U \sum_i n_{i\uparrow} n_{i\downarrow} \\
 & + \omega_0 \sum_i b_i^\dagger b_i + g \sum_{i\sigma} n_{i\sigma} (b_i^\dagger + b_i), \quad (1)
 \end{aligned}$$

\*jpedromend@gmail.com

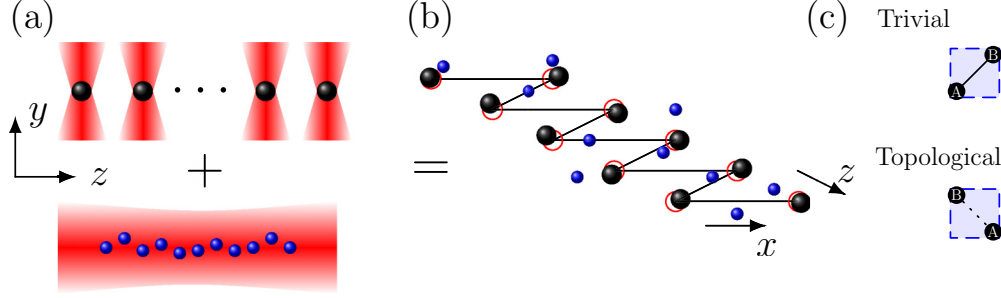


FIG. 1. (a) Red-detuned optical tweezers generating the Rydberg lattice (top) and state-insensitive trap for the ground-state atomic cloud (bottom). (b) The proposed platform. Strongly interacting Rydberg atoms (black balls) are trapped in an array of tweezers (red circles). The cloud neutral atoms (small blue balls) are placed in a periodic lattice potential due to the Rydberg chain. The lines are to guide the eyes. (c) The unit cells generating two lattice geometries with the base atoms labeled as A and B; the interactions shown here are strong (weak) for the trivial (topological) scenario.

where operators  $c_{i\sigma}$  annihilate an electron with spin  $\sigma$  at site  $i$  with  $n_{i\sigma} = c_{i\sigma}^\dagger c_{i\sigma}$  while  $b_i$  governs the local phonons with a single frequency  $\omega_0$ , and  $g$  is the onsite coupling strength. The model features surprisingly rich physics as phonon-induced interactions compete with the Hubbard term [16], leading to emergence of two insulating orders with a metallic phase appearing at their interplay [17–23]. The model can be easily extended, which considerably increases its complexity. For instance, one could modify the last term of Eq. (1) by introducing nonlocal electron-phonon coupling  $\mathcal{H}_{e\text{-ph}}$ . Within the second quantization, the extended version of the model is written as

$$\mathcal{H}_{e\text{-ph}} = \sum_{\mathbf{q}i} g_{\mathbf{q}i} (b_{\mathbf{q}}^\dagger + b_{\mathbf{q}}) \rho_i, \quad (2)$$

where  $\rho_i = \sum_{\sigma} n_{i\sigma}$  is the electron density and  $b_{\mathbf{q}}$  is the reciprocal representation of the local phonon  $b_i$ . While retaining a simple form, this term is rather general and can describe long-range couplings with nontrivial structure.

Furthermore, the phonon as well as electron dispersion can be replaced by a richer and more realistic structure. To showcase this, here we use a zig-zag configuration of Rydberg atoms with anisotropic interactions instead of a more standard cubic arrangement. This choice is motivated by a recent experiment [24] which emulated the physics of the Su-Schrieffer-Heeger model with topological edge states in a similar setup.

## II. TOPOLOGICAL RYDBERG LATTICE

In our approach the Rydberg atoms are constantly individually trapped by an array of harmonic potentials (optical tweezers) and interact with each other via dipolar interactions which can be induced with external electric field. As shown in Fig. 1(b), the traps are located at fixed positions forming a zig-zag chain in the  $x$ - $z$  plane. The atom positions are given by  $\mathbf{R}_{n\alpha}(t) = \mathbf{R}_n + \boldsymbol{\rho}_\alpha + \mathbf{u}_{n\alpha}(t)$ , where  $\mathbf{R}_n = n a \hat{\mathbf{z}}$  are the unit-cell positions,  $\boldsymbol{\rho}_\alpha$  labels the atoms within a cell with  $\alpha = A, B$  being the base atom label and  $n$  the cell position index, and  $\mathbf{u}_{n\alpha}(t)$  are the time-dependent displacements. The potential

energy is written as

$$V = \frac{1}{2} \sum_{n,\alpha} M_\alpha [v_n(\mathbf{R}_{n\alpha} - \bar{\mathbf{R}}_{n\alpha})]^2 + \sum_{\substack{nm\alpha\beta \\ (n,\alpha) \neq (m,\beta)}} \frac{V_{dd}}{|\mathbf{R}_{n\alpha,m\beta}|^3} [1 - 3(\hat{\mathbf{m}} \cdot \hat{\mathbf{R}}_{n\alpha,m\beta})^2], \quad (3)$$

where  $\bar{\mathbf{R}}_{n\alpha} = \mathbf{R}_n + \boldsymbol{\rho}_\alpha$  are the trap positions and  $\hat{\mathbf{R}}_{n\alpha,m\beta} = \hat{\mathbf{R}}_{n\alpha} - \hat{\mathbf{R}}_{m\beta}$ . The dipole moment orientation  $\hat{\mathbf{m}}$  is defined when the polar and azimuthal angles  $\theta$  and  $\phi$  are given. In a finite zig-zag chain with anisotropic couplings between the sites, there are two distinct geometries encoded in  $\boldsymbol{\rho}_\alpha$  [24,25] corresponding to forming pairs of dimers and leaving out two unpaired atoms at the chain edges. For the trivial configuration, we define  $\boldsymbol{\rho}_{A,B} = \mp \Delta/2 \hat{\mathbf{x}} \mp d/2 \hat{\mathbf{z}}$ , and  $\boldsymbol{\rho}_{A,B} = \mp \Delta/2 \hat{\mathbf{x}} \pm d/2 \hat{\mathbf{z}}$  for the topological one [see Fig. 1(c)]. Here, the length  $\Delta$  sets the distance between the two legs, while  $d$  is the spacing between the atoms in the same leg. For simplicity, we fix  $\mathbf{v}_n = \mathbf{v}$  with  $v_{x,y,z} = v$  and choose  $M_\alpha = M$ . Current state-of-the-art experiments enable an arbitrary three-dimensional setting of the tweezer traps with separations of the order of single  $\mu\text{m}$ . The trap frequencies can be varied as well and are typically in the  $\approx \text{kHz}$  regime. The interaction between the atoms depends on the choice of Rydberg states and can remain strong over the typical trap separation. Furthermore, it can be precisely tuned by using external electromagnetic fields, for instance by inducing and orienting the dipole moments [26].

Here for simplicity we use pure dipolar interactions, omitting the subleading quadrupolar and van der Waals terms, which would result in quantitative modifications of the phonon spectrum but offer additional tuning possibilities. If we choose  $\hat{\mathbf{m}} = (0, 1, 0)$  (out of the plane), the interactions become isotropic. Following [24], let us instead fix  $\theta = \theta_m = \cos^{-1}(1/\sqrt{3})$  where the interaction along the same sublattice vanishes as  $\hat{\mathbf{m}} \cdot \hat{\mathbf{R}}_{n\alpha,m\beta} = \hat{\mathbf{z}} = \cos \theta$  and  $\theta = \theta_m$ .

### A. Phonon spectrum

We now turn to the phonon structure of the Rydberg chain, expanding the potential energy to second order around the equilibrium configuration. The effective classical Hamiltonian

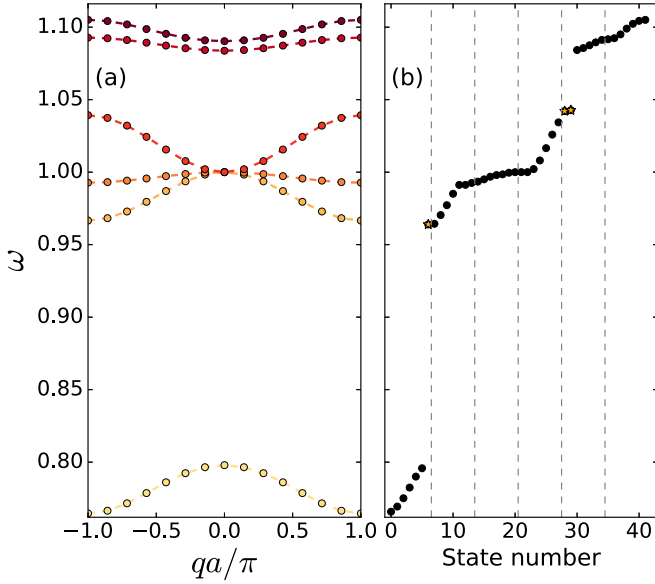


FIG. 2. The phonon dispersion relation for (a) the translationally invariant case and (b) the topological band structure of the finite chain for  $N = N_b N_c = 14$ ,  $d = 2$ ,  $\Delta = 1$ ,  $a = 2d$ ,  $\theta = \theta_m$ , and  $\phi = 0$ . The edge states are highlighted as yellow stars in panel (b).

is given by

$$H_{\text{eff}} = \sum_{n=1}^{N_c} \sum_{\alpha=1}^{N_b} \sum_{i=x,y,z} \frac{P_{n\alpha i}^2}{2M_\alpha} + \frac{1}{2} \sum_{nm} \sum_{\alpha\beta} \sum_{ij} u_{n\alpha i} D_{n\alpha i}^{m\beta j} u_{m\beta j}, \quad (4)$$

with  $N_c$  being the number of cells and  $N_b = 2$  the number of base atoms. The harmonic matrix  $D$  is given by the second derivatives of the potential at equilibrium. Interestingly, there is only one relevant interaction length scale  $\ell^5 = 3V_{dd}/Mv^2$  within this approximation. It is widely tunable by means of the trap frequencies as well as the choice of the Rydberg level, as the dipole-dipole interaction strength scales as  $n^4$ . We further express all other length scales describing the array geometry in units of  $\ell$  and energies in the corresponding characteristic units  $Mv^2\ell^2$ . Assuming an alkaline-earth atom and  $10^6$ -Hz trapping frequency, we obtain  $\ell \approx 10^4$  Bohr radii.

One can now obtain the phonon spectrum by diagonalizing the  $3N_c N_b \times 3N_c N_b$  harmonic matrix. On the other hand, if the translational invariance is applicable,  $D_{\alpha i}^{\beta j}(|\mathbf{R}_n - \mathbf{R}_m|) = D_{\alpha i}^{\beta j}(\mathbf{R}_p)$  and one can reduce the problem in the quasimomentum space to the  $3N_b \times 3N_b$  dynamical matrix [27]  $\tilde{D}_{\alpha i}^{\beta j}(\mathbf{q}) = \sum_n D_{\alpha i}^{\beta j}(\mathbf{R}_n) e^{i\mathbf{q} \cdot \mathbf{R}_n}$ . Here, for each of the  $N = N_b N_c$  allowed  $\mathbf{q}$  there are  $3N_b$  normal modes with frequencies  $\omega_j(\mathbf{q})$  and corresponding eigenvectors  $\xi_\alpha^{(j)}(\mathbf{q})$  obeying  $\sum_\alpha \xi_\alpha^{(j)}(\mathbf{q}) \cdot \xi_\alpha^{(j')}(\mathbf{q}) = \delta_{j,j'}$ , where  $j = 1, \dots, 3N_b$  and  $\alpha = 1, \dots, N_b$ . Due to the chosen geometry, in our example the quasimomentum is  $\mathbf{q} = q\hat{\mathbf{z}}$  as the system is quasi-one-dimensional. In the trivial or dimerized configuration, the finite chain has translational symmetry. Figure 2(a) shows its exemplary dispersion relation in the quasimomentum space. The system is widely tunable in terms of band geometry and shows a rich behavior which exhibits concavity changes and multiple band crossings, as shown in Fig. 3 for  $d = 1.5$  and  $2.5$  for the three highest

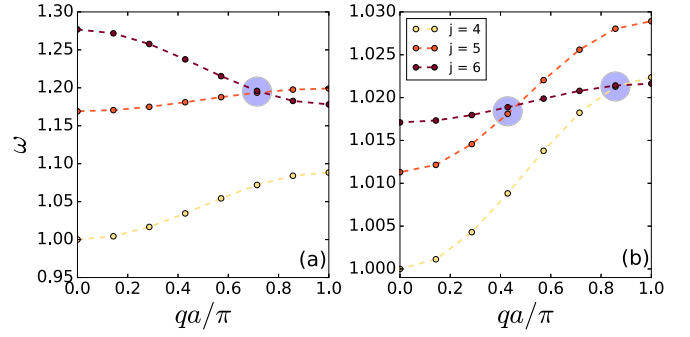


FIG. 3. Phonon spectrum of the three highest bands highlighting band crossings with a blue circle. As an example, we show (a)  $d = 1.5$  and (b)  $d = 2.5$ , with  $N = N_b N_c = 14$ ,  $\Delta = 1$ ,  $a = 2d$ ,  $\theta = \theta_m$ , and  $\phi = 0$ .

phonon modes. Furthermore, both highest and lowest bands are changing their concavity with varying the distance  $d$ . We show in Fig. 4 two examples of such concavity change. It is demanding to find numerically the critical value at which the concavity changes, as one encounters instabilities in the atom equilibrium positions. As demonstrated in the figure, it is located between  $d = 1.65$  and  $1.85$  for both the first and the last band. For the topological configuration, the translational invariance can no longer be assumed. In Fig. 2(b) we show the dispersion relation calculated from direct diagonalization of the harmonic matrix. We observe three points which are disconnected from the bands: one in the first and two in the fifth band, which we associate with the edge states. It is important to note that even for larger values of  $N$ , we still see only these three disconnected points.

### B. Local phonon couplings

To gain more insight into the phonon mode structure, following [28] we can rewrite the phonon Hamiltonian in terms of local phonon operators:

$$H = \frac{1}{2} \sum_{nmj} [h_{nm}^{ij} (b_{n,i}^\dagger b_{m,j} + b_{n,i} b_{m,j}^\dagger) + g_{nm}^{ij} (b_{n,i} b_{m,j} + b_{n,i}^\dagger b_{m,j}^\dagger)], \quad (5)$$

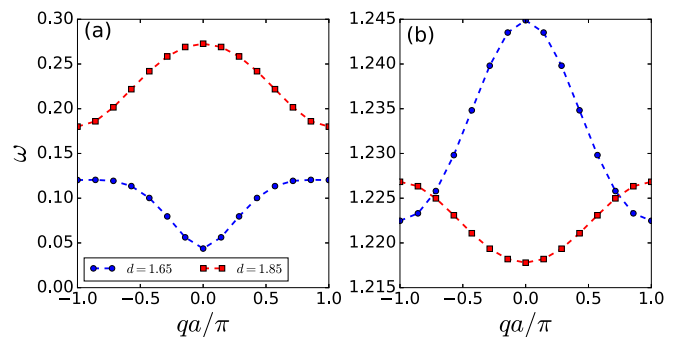


FIG. 4. Phonon spectrum of the (a) first band and (b) last band for  $d = 1.65$  and  $1.85$ . We can see that there is a concavity change by varying  $d$  between the values shown. Here we set  $N = N_b N_c = 14$ ,  $\Delta = 1$ ,  $a = 2d$ ,  $\theta = \theta_m$ , and  $\phi = 0$ .

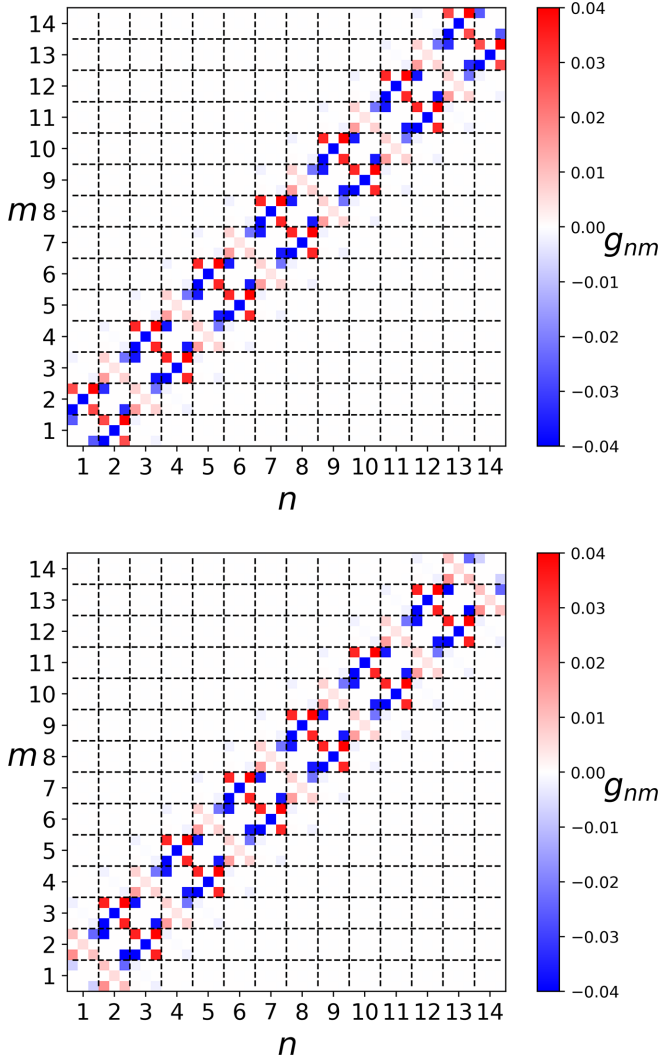


FIG. 5. Elements of the interaction matrix  $g$  for trivial (top) and topological (bottom) configurations. We saturated the colors for a better visualization. The interactions for  $|n - m| = 1$  are alternating between strong and weak. Here we fixed  $N = 14$ ,  $d = 2$ ,  $\Delta = 1$ ,  $a = 2d$ ,  $\theta = \theta_m$ , and  $\phi = 0$ .

where the displacements are quantized as  $u_{n,i} = \sqrt{\frac{1}{2M\Omega_{n,i}}}(b_{n,i} + b_{n,i}^\dagger)$ , with the local frequency  $\Omega_{n,i}$  defined as  $D_{nn}^{ii} = M\Omega_{n,i}^2$ . Furthermore, the couplings are given by the matrix  $g$  with  $g_{nm}^{jj} = (1 - \delta_{nm}\delta_{ij})D_{nm}^{ij}/2M\sqrt{\Omega_{n,i}\Omega_{m,j}}$  and  $h_{nm}^{ij} = \delta_{nm}\delta_{ij}\Omega_{n,i} + g_{nm}^{ij}$ , with  $n, m \in [0, N]$  now being the overall atom index where  $N = N_b N_c$  [see Fig. 6(d)]. The  $g$  matrix has  $9N^2$  elements describing nine possible couplings between each pair of lattice sites in  $3 \times 3$  directions. We show in Fig. 5 the elements of the interaction matrix  $g$  in a grid. Each box shows nine matrix elements between the unit cells. In this figure, it is possible to see the staggered nature of the interactions between cells. The main difference between topological and trivial is whether the edges are weakly or strongly interacting with the bulk.

For visualization we also show in Fig. 6(c) the quantity  $J(|n - m|) = \sum_{ij} g_{nm}^{ij}$  for distinct values of  $|n - m|$  and  $d$ .

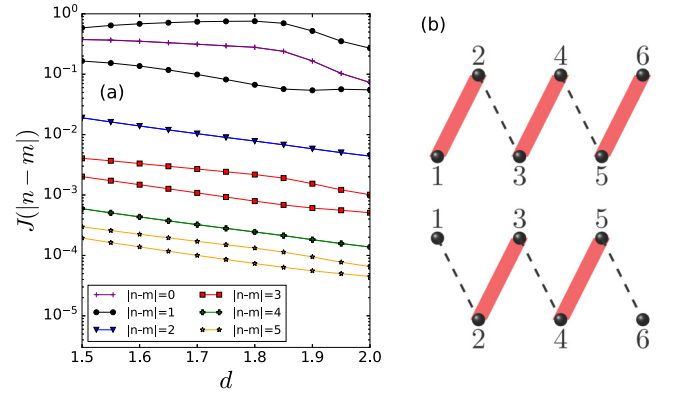


FIG. 6. (a) Couplings between local phonons as a function of  $d$  for different pairs  $n$  and  $m$  for  $N = 14$ ,  $d = 2$ ,  $\Delta = 1$ ,  $a = 2d$ ,  $\theta = \theta_m$ , and  $\phi = 0$ . (b) Trivial and topological geometries where the lines depict the strong (red thick line) and weak (black dashed line) links (see text).

The terms with odd  $|n - m|$  describe the overall coupling between two different legs for two cases corresponding to the majority of weak or strong bonds between the sites. Such staggered nature can be directly associated with the Su-Schrieffer-Heeger model. Even  $|n - m|$  values provide the interactions along the same sublattice [see Fig. 6(d)] which do not vanish even at the magic angle  $\theta_m$  due to displacements of atoms from equilibrium. As the trap separation  $d$  decreases, interactions in general become stronger. However, the intracell couplings feature a maximum near  $d \approx 1.8$ , which is related to the system geometry and coincides with the concavity change of the lowest band, indicating the presence of geometric frustration.

We have so far demonstrated that phonons in Rydberg atom arrays are capable of simulating complex solid-state systems with highly tunable band structure. Extension to a two-dimensional setup would enable the occurrence of chiral edge states. Implementation of driving into the system with lasers can induce additional nonequilibrium dynamics [29].

### III. GROUND-STATE ATOMS

We proceed to adding the second subsystem composed of ground-state atoms. Their van der Waals interaction with the Rydberg atoms can be described by a Fermi pseudopotential with tunable magnitude  $g_{cp}$ , omitting off-diagonal terms which are small due to low dipole moment of the ground electronic state [26,30]. For the whole array,  $H_{\text{Ry-a}} = \sum_{n,m} \sum_{\alpha} V_{\text{Ry-a}}(\mathbf{r}_n - \mathbf{R}_{m\alpha})$ . This can be expanded in power series in Rydberg displacements  $u$ , providing a constant term which forms the periodic potential for the atoms while the atom-phonon interaction is encoded in the first-order term. Within the tight-binding approximation, the bare atomic Hamiltonian without phonons is described by the Hubbard model

$$\mathcal{H}_a = -t \sum_{(i,j)\sigma} (c_{i\sigma}^\dagger c_{j\sigma} + \text{H.c.}) + U \sum_i n_{i\uparrow} n_{i\downarrow}, \quad (6)$$



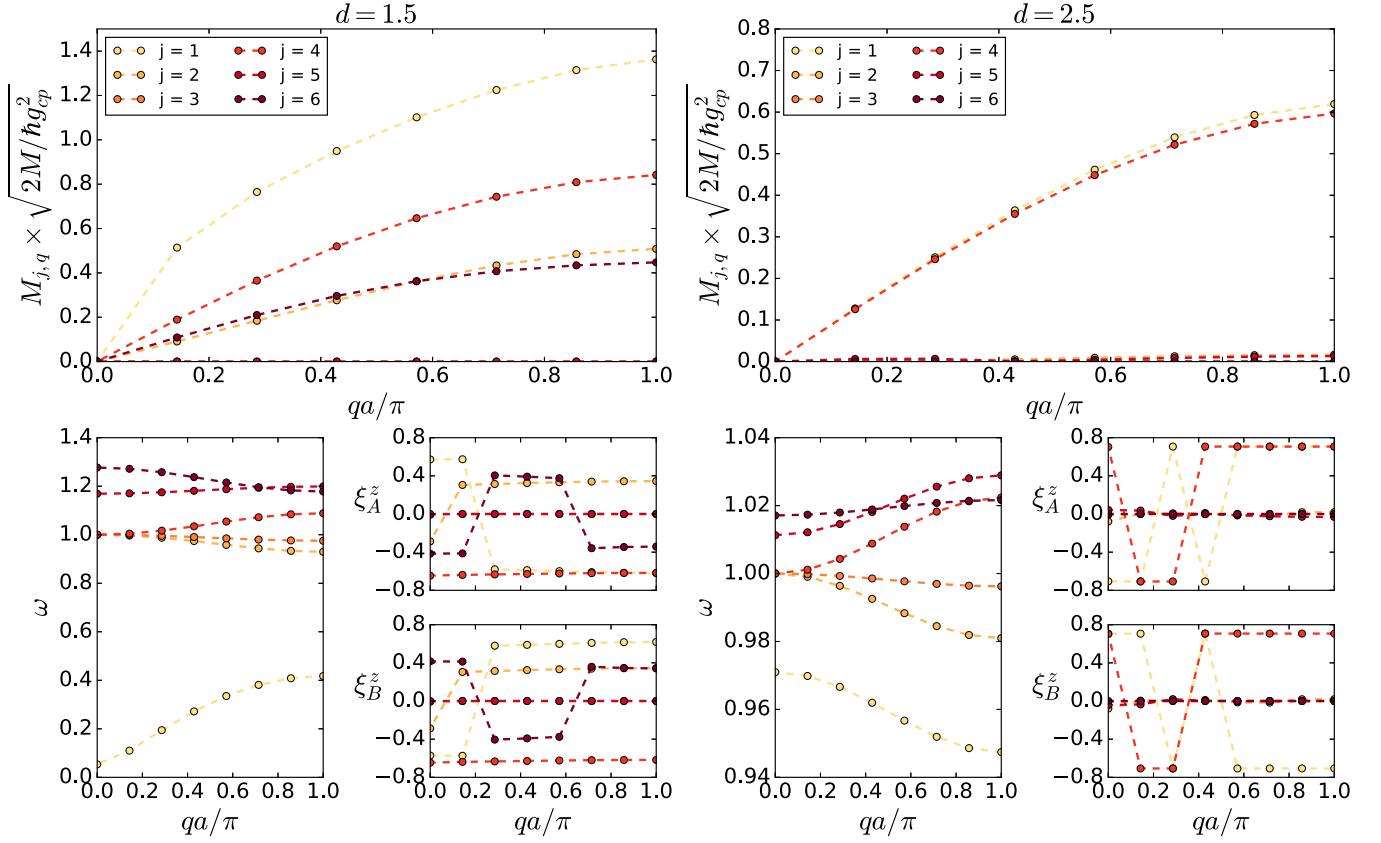


FIG. 7. Interaction strength  $M_{j,q}$  for  $d = 1.5$  and  $d = 2.5$ . We show two examples where there is a clear distinction between multiband and two-band regimes. The corresponding phonon spectra and eigenvector component in the  $z$  direction are shown in the bottom panels. Here  $N = 14$ ,  $\Delta = 1$ ,  $a = 2d$ ,  $\theta = \theta_m$ , and  $\phi = 0$ .

where  $t$  is the hopping strength and  $U$  is the Hubbard interaction.

#### IV. THE ATOM-PHONON HAMILTONIAN

The atom-phonon Hamiltonian is obtained by the second quantization of the phonon relevant part of the interaction Hamiltonian,  $H_{\text{Ry-}a}^{(1)}$ , as shown in the Appendix B. For our neutral atomic system, we restrict to the lowest Bloch band and tight-binding approximation. We used a Gaussian approximation for the lattice Wannier functions, which for composite lattices may need to be modified [31–33] but does not qualitatively impact our results. Overall, the atom-phonon Hamiltonian is then given by

$$\mathcal{H}_{a\text{-ph}} = \sum_{\mathbf{q}, \mathbf{k}, j, \sigma} \frac{1}{\sqrt{N}} M_{j,\mathbf{q}} (b_{j,\mathbf{q}} + b_{j,-\mathbf{q}}^\dagger) c_{\mathbf{k}+\mathbf{q},\sigma}^\dagger c_{\mathbf{k},\sigma}, \quad (7)$$

where the interaction strength is given by

$$M_{j,\mathbf{q}} = \sum_{\alpha} \sqrt{\frac{\hbar g_{cp}^2}{2M_{\alpha} \omega_j(\mathbf{q})}} \mathbf{q} \cdot \xi_{\alpha}^{(j)}(\mathbf{q}) e^{-i\mathbf{q} \cdot \rho_{\alpha}} \rho_0(\mathbf{q}), \quad (8)$$

with  $\rho_0 = \int d\mathbf{r} e^{i\mathbf{q} \cdot \mathbf{r}} |\phi_0(\mathbf{r})|^2$  and  $\phi_0(\mathbf{r})$  being the Wannier function of the lowest Bloch band.

In a zig-zag chain where  $\mathbf{q} = q\hat{\mathbf{z}}$ , the dot product in  $M_{j,\mathbf{q}}$  restricts the couplings and as a result transverse states without a  $z$  component do not interact with the atoms. We observe that the interaction strength is highly dependent on

the phonon energy and structure. Indeed, the other functions appearing in Eq. (8) will mostly affect the overall strength of the coupling profile. In order to design the desired interaction between ground-state atoms and phonons one thus needs to focus on the phonon part. The proposed Rydberg lattice setup turns out to be perfect for such a situation since it is a rich and highly controllable platform as discussed earlier.

In Fig. 7 we show two exemplary situations in which the coupling term crosses over from a two-band to a multiband structure. Its overall magnitude can be easily controlled independently by manipulating the Rydberg-atom interaction strength. For a better understanding, we show in the bottom panels of Fig. 7 the phonon spectrum and the  $z$  component of the corresponding states. As we can see, when  $d$  is big compared with the other lengths, only the first and fourth band are generating noticeable oscillations in the  $z$  direction. Decreasing the distance between the Rydberg atoms, other bands also acquire vibrational components along the  $z$  axis. This is the limitation of the quasi-one-dimensional platform as only longitudinal phonons can contribute. In addition, the atom-phonon coupling to the first phonon band shows a non-monotonic behavior with  $d$  due to the change in the band shape. As we can see in Fig. 8, from  $d = 1.5$  to  $1.65$  the band is flattening, which increases the interaction strength due to the phonon energy being in the denominator. After the concavity changing transition, the band starts to widen and increase in amplitude again.

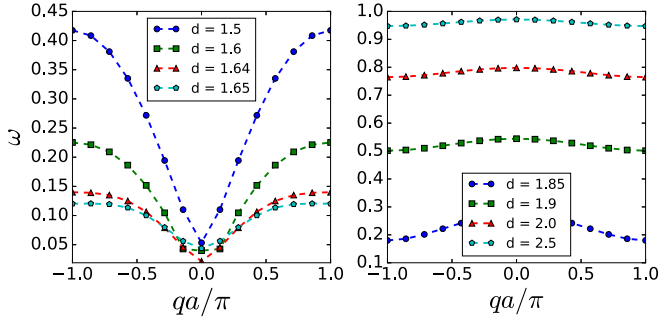


FIG. 8. Phonon spectrum of the first band and for many values of  $d$ . In the left panel, the phonon frequency is decreasing with an increasing  $d$ , while in the right panel it is the opposite case. Here  $N = 14$ ,  $\Delta = 1$ ,  $a = 2d$ ,  $\theta = \theta_m$ , and  $\phi = 0$ .

## V. DISCUSSION

As discussed above, the whole system is described by an extended Hubbard-Holstein model

$$\begin{aligned} \mathcal{H}_{\text{eff}} = & -t \sum_{(i,j)\sigma} (c_{i\sigma}^\dagger c_{j\sigma} + \text{H.c.}) + U \sum_i n_{i\uparrow} n_{i\downarrow} \\ & + \sum_{j,\mathbf{q}} \hbar\omega_j(\mathbf{q}) b_{j,\mathbf{q}}^\dagger b_{j,\mathbf{q}} \\ & + \sum_{\mathbf{q},\mathbf{k},j,\sigma} \frac{1}{\sqrt{N}} M_{j,\mathbf{q}} (b_{j,\mathbf{q}} + b_{j,-\mathbf{q}}^\dagger) c_{\mathbf{k}+\mathbf{q},\sigma}^\dagger c_{\mathbf{k},\sigma}, \quad (9) \end{aligned}$$

with nontrivial phonon structure including the possibility for topological bands and nonlocal couplings. Phonon-induced interactions can induce long-range attraction between the fermions and enhance the formation of pairs and conductivity. While one can study the limiting cases of weak or very strong coupling analytically, e.g., by means of a generalized Lang-Firsov transformation [11,16,20,22], we stress that due to the competition of terms the problem calls for a thorough numerical study in order to verify and interpret the quantum simulator output.

### A. Experimental feasibility

We now argue that each quantity in (7) can be tuned with some degree of independence and can reach several kHz, providing sufficiently fast dynamics to operate within the Rydberg atom lifetime. Let us first discuss the parameter values achievable in current experiments. For simplicity, here we work with a quasi-one-dimensional chain with linear configuration of Rydberg atoms of equidistant separation  $d$ . The van der Waals  $C_6$  coefficient between the ground-state and Rydberg atom grows with the principal quantum number as  $\approx n^5$  [34], in contrast to  $n^{11}$  scaling for both atoms excited [35]. Still, this leads to the characteristic range of the potential  $R_6 = (2\mu C_6/\hbar^2)^{1/4}$  [36] being widely tunable. Assuming a  $\text{Rb}^*\text{-Li}$  pair one obtains  $R_6 \approx 300$  nm already for  $n \approx 50$ , meaning that interactions within the lattice are strong.

One can then proceed with estimation of the extended Hubbard-Holstein Hamiltonian parameters. Assuming tight-binding approximation, we obtain the tunneling coefficient [11]  $t \approx 4E_r^2 d/\pi^2 g_{cp}$  where  $E_r = \frac{\pi^2 \hbar^2}{2md^2}$  and  $m$  is the atomic

mass. Note that in order to make  $t$  appropriately large, using light atoms such as lithium seems to be the most convenient option. Meanwhile,  $M_{a\text{-ph}} \propto \sqrt{\frac{\hbar g_{cp}^2}{2M\omega}}$  with  $M$  being the mass of the Rydberg atoms. Even though the coupling term  $\propto g_{cp}$  while  $t \propto 1/g_{cp}$ , tuning the spacing and tweezers trap frequency allows for manipulating the parameters independently. The Hubbard  $U$  term is independently tunable using a magnetic Feshbach resonance [36]. Assuming  $d \approx 1 \mu\text{m}$  and  $g_{cp} \approx 10^4$  Hz, we obtain  $M_{a\text{-ph}}$  in the same range and  $t \approx 3$  kHz, comparable to other energy scales. For high enough  $n$  all parameters will exceed the Rydberg level decay rate  $\Gamma$ , as highly excited states can reach lifetimes of the order of 1 ms.

Finally, a reliable quantum simulator requires initializing the system with high fidelity. This may require some optimization steps. For instance, direct excitation of a chain of atoms trapped in tweezers to a Rydberg state at small separation is a nontrivial task due to the Rydberg blockade phenomenon [6]. In order to circumvent it, one can either utilize optimal control protocols [37,38] or excite the atoms further away from each other and then bring them to the designated positions. For alkali-metal atoms, this protocol can be challenging [39], but alkaline-earth-based setups [14] can offer an advantage here. Similarly, loading the lattice efficiently is desired due to the finite lifetime of the system. Here we would suggest to prepare the ground-state atoms in a separate set of optical tweezers and subsequently release them into the lattice.

### B. Quantum simulation prospects

Experimentally, the system provides a number of possible measurements such as time-of-flight and *in situ* imaging of atoms, as well as phonon state tomography of the chain. Studying the dynamics after a quench or under driving should not impose any additional challenge.

We also notice that a class of extended Hubbard-Holstein models could also be studied with a possibly simpler system in the spirit of variational quantum simulation [40,41]. In this scenario one would use an ansatz for the phonon part in order to calculate the effective fermionic Hamiltonian classically, and then find the ground state of the reduced system by implementing it in experiment and obtaining a new candidate phonon state for the next iteration.

## VI. CONCLUSIONS

We have proposed a highly tunable experimental platform for simulation of compound quantum systems. It can be utilized for exploration of phase diagrams of extended Hubbard models in various geometric arrangements, possibly to study the onset of bipolaronic superconductivity. In the future, extensions to two- and three-dimensional structures and designing the system to exhibit flat bands and edge states seem particularly promising [25,42–46], with exciting prospects for nonequilibrium dynamics and phonon driving related to recent breakthrough results on transient superconductivity [47,48].

### ACKNOWLEDGMENTS

This work was supported by the Polish National Agency for Academic Exchange (NAWA) via the Polish Returns 2019 program.

### APPENDIX A: LOCAL PHONON INTERACTIONS

Below we give some analytical details and important numerical results not shown in the main text. In order to obtain a good picture of the Rydberg-Rydberg interactions in the harmonic approximation, we move to the local phonon study, following Bissbort *et al.* [28].

We can rewrite the phonon Hamiltonian as

$$\begin{aligned} H &= \sum_{n,i} \frac{P_{n,i}^2}{2M_n} + \frac{1}{2} \sum_{n,m,i,j} u_{n,i} D_{nm}^{ij} u_{m,j} \\ &= \frac{1}{2} \sum_{n,i} \left( \frac{P_{n,i}^2}{M_n} + D_{nm}^{ii} u_{n,i}^2 \right) + \frac{1}{2} \sum_{\substack{n,m,i,j \\ (n,i) \neq (m,j)}} u_{n,i} D_{nm}^{ij} u_{m,j}. \end{aligned} \quad (\text{A1})$$

We can second quantize it defining

$$u_{n,i} = \sqrt{\frac{1}{2M_n \Omega_{n,i}}} (b_{n,i} + b_{n,i}^\dagger), \quad (\text{A2})$$

$$P_{n,i} = i \sqrt{\frac{2M_n \Omega_{n,i}}{2}} (b_{n,i}^\dagger - b_{n,i}), \quad (\text{A3})$$

where  $D_{nm}^{ii} = M_n \Omega_{n,i}^2$ . The first term in Eq. (A1) is a collection of local harmonic oscillators  $\frac{1}{2} \sum_{n,i} \Omega_{n,i} (b_{n,i}^\dagger b_{n,i} + b_{n,i} b_{n,i}^\dagger)$ . The second term represents the interaction part of the Hamiltonian:

$$\begin{aligned} \frac{1}{2} \sum_{\substack{n,m,i,j \\ (n,i) \neq (m,j)}} \frac{D_{nm}^{ij}}{2M_n \sqrt{\Omega_{n,i} \Omega_{m,j}}} (b_{n,i} b_{m,j} + b_{n,i} b_{m,j}^\dagger \\ + b_{n,i}^\dagger b_{m,j} + b_{n,i}^\dagger b_{m,j}^\dagger). \end{aligned} \quad (\text{A4})$$

The full phonon Hamiltonian can be written in a more convenient way:

$$H = \frac{1}{2} \sum_{nmij} [h_{nm}^{ij} (b_{n,i}^\dagger b_{m,j} + b_{n,i} b_{m,j}^\dagger) + g_{nm}^{ij} (b_{n,i} b_{m,j} + b_{n,i}^\dagger b_{m,j}^\dagger)], \quad (\text{A5})$$

where

$$g_{nm}^{jj} = \frac{(1 - \delta_{nm} \delta_{ij}) D_{nm}^{jj}}{2M_n \sqrt{\Omega_{n,i} \Omega_{m,j}}}, \quad (\text{A6})$$

$$h_{nm}^{ij} = \delta_{nm} \delta_{ij} \Omega_{n,i} + g_{nm}^{ij}. \quad (\text{A7})$$

### APPENDIX B: ATOM-PHONON COUPLING

The details about the analytical derivations of the atom-phonon Hamiltonian can be found in this section. Despite the textbook character, there are important details specific to the problem.

The interaction between the two different species is given by

$$H_{\text{Ry-a}} = \sum_{n,m} \sum_{\alpha=1}^{N_b} V_{\text{Ry-a}}(\mathbf{r}_n - \mathbf{R}_{m\alpha}). \quad (\text{B1})$$

This can be expanded in power series in Rydberg displacements  $u$ :

$$\begin{aligned} H_{\text{Ry-a}} &= \sum_n \sum_{m,\alpha} V_{\text{Ry-a}}(\mathbf{r} - \bar{\mathbf{R}}_{n\alpha} - \mathbf{u}_{m\alpha}) \\ &\approx \sum_n \sum_{m,\alpha} V_{\text{Ry-a}}(\mathbf{r}_n - \bar{\mathbf{R}}_{n\alpha}) \\ &\quad - \sum_n \sum_{m,\alpha} \mathbf{u}_{m\alpha} \cdot \nabla_{\mathbf{R}_{m\alpha}} V_{\text{Ry-a}}(\mathbf{r}_n - \mathbf{R}_{m\alpha}) \Big|_{\bar{\mathbf{R}}_{n\alpha}} \\ &\equiv H_{\text{Ry-a}}^{(0)} + H_{\text{Ry-a}}^{(1)}, \end{aligned} \quad (\text{B2})$$

with  $\bar{\mathbf{R}}_{n\alpha} = \mathbf{R}_n + \boldsymbol{\rho}_\alpha$ . The constant term in  $\mathbf{u}_{m\alpha}$  forms the periodic potential and it is already taken into account in  $\mathcal{H}_a$ . In that way, the atom-phonon interaction is encoded in the first-order term. The constant part will be neglected from here. We will also neglect higher-order terms,  $\mathcal{O}(u^2)$ . The gradient can be straightforwardly evaluated writing  $V_{\text{Ry-a}}(\mathbf{r})$  in the reciprocal space as  $V_{\text{Ry-a}}(\mathbf{r} - \mathbf{R}_{m\alpha}) = \frac{1}{V} \sum_{\mathbf{Q}} e^{i\mathbf{Q} \cdot (\mathbf{r} - \mathbf{R}_{m\alpha})} V_{\mathbf{Q}}$ :

$$\nabla_{\mathbf{R}_{m\alpha}} V_{\text{Ry-a}}(\mathbf{r}_n - \mathbf{R}_{m\alpha}) \Big|_{\bar{\mathbf{R}}_{n\alpha}} = \frac{-i}{V} \sum_{\mathbf{Q}} \mathbf{Q} e^{i\mathbf{Q} \cdot (\mathbf{r} - \bar{\mathbf{R}}_{n\alpha})} V_{\mathbf{Q}}. \quad (\text{B3})$$

Thus, we can write the second quantized atom-phonon Hamiltonian [49]:

$$\mathcal{H}_{\text{a-ph}} = \sum_{b,k,\sigma} \sum_{b',k',\sigma'} \langle b, k, \sigma | H_{\text{Ry-a}}^{(1)} | b', k', \sigma' \rangle c_{b,k,\sigma}^\dagger c_{b',k',\sigma'}, \quad (\text{B4})$$

where the relevant indices are the Bloch band  $b$ , momentum  $\mathbf{k}$ , and spin  $\sigma$ . The coefficients are given by

$$\begin{aligned} \langle b, k, \sigma | H_{\text{Ry-a}}^{(1)} | b', k', \sigma' \rangle &= - \int d\mathbf{r} \Psi_{b,k,\sigma}^*(\mathbf{r}) \\ &\quad \times \sum_{n,\alpha} \mathbf{u}_{n\alpha} \cdot \nabla_{\mathbf{R}_{n\alpha}} V_{\text{Ry-a}}(\mathbf{r} - \mathbf{R}_{n\alpha}) \Big|_{\bar{\mathbf{R}}_{n\alpha}} \Psi_{b',k',\sigma'}(\mathbf{r}) \\ &= \frac{i}{V} \sum_{n,\alpha,\mathbf{Q}} \mathbf{Q} \cdot \mathbf{u}_{n\alpha} e^{-i\mathbf{Q} \cdot \bar{\mathbf{R}}_{n\alpha}} V_{\mathbf{Q}} \int d\mathbf{r} \Psi_{b,k,\sigma}^*(\mathbf{r}) e^{i\mathbf{Q} \cdot \mathbf{r}} \Psi_{b',k',\sigma'}(\mathbf{r}). \end{aligned} \quad (\text{B5})$$

The second quantized displacement operator can be written in terms of its Fourier transform:

$$\mathbf{u}_{n\alpha} = \sum_{\mathbf{q}} \sum_{j=1}^{3N_b} \sqrt{\frac{\hbar}{2M_\alpha \omega_j(\mathbf{q})}} \boldsymbol{\xi}_\alpha^{(j)}(\mathbf{q}) (b_{j,\mathbf{q}} + b_{j,-\mathbf{q}}^\dagger) \frac{e^{i\mathbf{q} \cdot \mathbf{R}_n}}{\sqrt{N}}, \quad (\text{B6})$$

where  $\omega_j$  and  $\boldsymbol{\xi}_\alpha^{(j)}$  are the eigenvalues and eigenvectors of the dynamical matrix,  $j$  is the phonon band index, and  $N = N_b N_c$ . We can write  $e^{-i\mathbf{Q} \cdot \bar{\mathbf{R}}_{n\alpha}} = e^{-i\mathbf{Q} \cdot \mathbf{R}_n} e^{-i\mathbf{Q} \cdot \boldsymbol{\rho}_\alpha}$ , and in Eq. (B5) will appear  $\sum_n e^{i(\mathbf{q} - \mathbf{Q}) \cdot \mathbf{R}_n} = N \delta_{\mathbf{q},\mathbf{Q}}$ . The atom-phonon Hamil-

tonian is written as

$$\begin{aligned} \mathcal{H}_{a\text{-ph}} &= \frac{i}{\sqrt{N}} \sum_{\mathbf{q},j} \sum_{b,k,\sigma} \sum_{b',k',\sigma'} \sqrt{\frac{\hbar}{2M_\alpha \omega_j(\mathbf{q})}} \mathbf{q} \cdot \xi_\alpha^{(j)}(\mathbf{q}) e^{-i\mathbf{q} \cdot \rho_\alpha} \\ &\quad \times V_{\mathbf{q}} \alpha_{q,b,k,\sigma,b',k',\sigma'} (b_{j,\mathbf{q}} + b_{j,-\mathbf{q}}^\dagger) c_{b,k,\sigma}^\dagger c_{b',k',\sigma'} \\ &= \sum_{\mathbf{q},j} \sum_{b,k,\sigma} \sum_{b',k',\sigma'} \frac{1}{\sqrt{N}} M_{q,j,b,k,\sigma,b',k',\sigma'} \\ &\quad \times (b_{j,\mathbf{q}} + b_{j,-\mathbf{q}}^\dagger) c_{b,k,\sigma}^\dagger c_{b',k',\sigma'}, \end{aligned} \quad (\text{B7})$$

where we defined

$$\alpha_{q,b,k,\sigma,b',k',\sigma'} = \frac{1}{\Omega} \int d\mathbf{r} \Psi_{b,k,\sigma}^*(\mathbf{r}) e^{i\mathbf{q} \cdot \mathbf{r}} \Psi_{b',k',\sigma'}(\mathbf{r}), \quad (\text{B8})$$

and  $\Omega = V/N$ . Let us evaluate the overlap integral above in terms of the Wannier functions within some approximations. First, consider the potential is independent of the spin, so  $\sigma = \sigma'$  and then  $\alpha$  is independent of the spin. In terms of the Wannier functions,

$$\Psi_{b,k}(\mathbf{r}) = \frac{1}{\sqrt{N}} \sum_{\mathbf{R}} e^{i\mathbf{k} \cdot \mathbf{R}} \phi_b(\mathbf{r} - \mathbf{R}), \quad (\text{B9})$$

we can evaluate  $\alpha$ :

$$\begin{aligned} \Omega \alpha_{q,b,k,b',k'} &= \int d\mathbf{r} \Psi_{b,k}^*(\mathbf{r}) e^{i\mathbf{q} \cdot \mathbf{r}} \Psi_{b',k'}(\mathbf{r}) \\ &= \frac{1}{N} \sum_{\mathbf{R}, \mathbf{R}'} e^{-i\mathbf{k} \cdot \mathbf{R}} e^{i\mathbf{k}' \cdot \mathbf{R}'} \int d\mathbf{r} \\ &\quad \times e^{i\mathbf{q} \cdot \mathbf{r}} \phi_b^*(\mathbf{r} - \mathbf{R}) \phi_{b'}(\mathbf{r} - \mathbf{R}'). \end{aligned} \quad (\text{B10})$$

Within the tight-binding approximation, terms  $\mathbf{R} \neq \mathbf{R}'$  are vanishing:

$$\Omega \alpha_{q,b,k,b',k'} = \frac{1}{N} \sum_{\mathbf{R}} e^{i(\mathbf{k}' - \mathbf{k}) \cdot \mathbf{R}} \int d\mathbf{r} e^{i\mathbf{q} \cdot \mathbf{r}} \phi_b^*(\mathbf{r} - \mathbf{R}) \phi_{b'}(\mathbf{r} - \mathbf{R}). \quad (\text{B11})$$

In the single band approximation, we fix  $b = b' = 0$ :

$$\begin{aligned} \Omega \alpha_{q,k,k'} &= \frac{1}{N} \sum_{\mathbf{R}} e^{i(\mathbf{k}' - \mathbf{k}) \cdot \mathbf{R}} \int d\mathbf{r} e^{i\mathbf{q} \cdot \mathbf{r}} |\phi_0(\mathbf{r} - \mathbf{R})|^2 \\ &= \frac{1}{N} \sum_{\mathbf{R}} e^{i(\mathbf{k}' - \mathbf{k}) \cdot \mathbf{R}} e^{i\mathbf{q} \cdot \mathbf{R}} \int d\mathbf{r} e^{i\mathbf{q} \cdot \mathbf{r}} |\phi_0(\mathbf{r})|^2, \end{aligned} \quad (\text{B12})$$

but  $\frac{1}{N} \sum_{\mathbf{R}} e^{i(\mathbf{q} + \mathbf{k}' - \mathbf{k}) \cdot \mathbf{R}} = \delta_{\mathbf{q} + \mathbf{k}', \mathbf{k}}$  and we define  $\rho_0 = \int d\mathbf{r} e^{i\mathbf{q} \cdot \mathbf{r}} |\phi_0(\mathbf{r})|^2$ . The atom-phonon Hamiltonian takes the simple form

$$\mathcal{H}_{a\text{-ph}} = \sum_{\mathbf{q},k,j,\sigma} \frac{1}{\sqrt{N}} M_{j,\mathbf{q}} (b_{j,\mathbf{q}} + b_{j,-\mathbf{q}}^\dagger) c_{\mathbf{k}+\mathbf{q},\sigma}^\dagger c_{\mathbf{k},\sigma}, \quad (\text{B13})$$

where the interaction strength is given by

$$M_{j,\mathbf{q}} = \sum_{\alpha} \sqrt{\frac{\hbar}{2M_\alpha \omega_j(\mathbf{q})}} \mathbf{q} \cdot \xi_\alpha^{(j)}(\mathbf{q}) e^{-i\mathbf{q} \cdot \rho_\alpha} V_{\mathbf{q}} \rho_0(\mathbf{q}). \quad (\text{B14})$$

Here we set  $\Omega = 1$  and get rid of the  $i$  by a rotation (global phase transformation).

In a zig-zag chain where  $\mathbf{q} = q\hat{\mathbf{z}}$ , the dot product in  $M_{j,\mathbf{q}}$  restricts the couplings and as a result transverse states without a  $z$  component do not interact with the atoms:

$$\mathcal{H}_{a\text{-ph}} = \sum_{q,k,j,\sigma} \frac{1}{\sqrt{N}} M_{j,q} (b_{j,q} + b_{j,-q}^\dagger) c_{k+q,\sigma}^\dagger c_{k,\sigma}, \quad (\text{B15})$$

with

$$M_{j,q} = \sum_{\alpha} \sqrt{\frac{\hbar g_{cp}^2}{2M_\alpha \omega_j(q)}} q \xi_{\alpha,z}^{(j)}(q) e^{-iq\rho_\alpha^z} \rho_0(q), \quad (\text{B16})$$

where a Fermi pseudopotential with magnitude  $g_{cp}$  was taken into account for  $V_q$ . Here we used the Orner *et al.* approximation for the lattice Wannier functions [11], which for composite lattices may need to be modified [31–33] but does not qualitatively impact our results. Thus,

$$\rho_0(q) = \int d\mathbf{r} e^{iqz} |\phi_0(\mathbf{r})|^2 \approx \frac{8\pi^2 \sin(qd/2)}{4\pi^2 qd - q^3 d^3}. \quad (\text{B17})$$

Therefore, we aim to study the interactions described by the following equation:

$$\sqrt{\frac{2M}{\hbar g_{cp}^2}} M_{j,q} = \frac{q\rho_0(q)}{\sqrt{\omega_j(q)}} \sum_{\alpha} |\xi_{\alpha,z}^{(j)}(q)| e^{-iq\rho_\alpha^z}, \quad (\text{B18})$$

where  $M_\alpha = M$ . The interaction strength inversely depends on the eigenvalues  $\omega_j$  and directly depends on the  $z$  component of the eigenvectors  $\xi_{\alpha,z}^{(j)}$ , while  $\rho_0$  and  $e^{-iq\rho_\alpha^z}$  will just shape the interaction pattern. In other words, to understand the interaction behavior, one needs both  $\omega_j$  and  $\xi_{\alpha,z}^{(j)}$ . If we change  $\xi_{\alpha,z}^{(j)} \rightarrow -\xi_{\alpha,z}^{(j)}$  (for all  $j$ ), the orthonormality condition still holds. That is why there is a modulus in Eq. (B18).

- [1] J. I. Cirac and P. Zoller, *Nat. Phys.* **8**, 264 (2012).
- [2] I. M. Georgescu, S. Ashhab, and F. Nori, *Rev. Mod. Phys.* **86**, 153 (2014).
- [3] J. Fraxanet, T. Salamon, and M. Lewenstein, [arXiv:2204.08905](https://arxiv.org/abs/2204.08905).
- [4] E. Altman, K. R. Brown, G. Carleo, L. D. Carr, E. Demler, C. Chin, B. DeMarco, S. E. Economou, M. A. Eriksson, Kai-Mei C. Fu, M. Greiner, K. R. A. Hazzard, R. G. Hulet, A. J. Kollár, B. L. Lev, M. D. Lukin, R. Ma, X. Mi, S. Misra, C. Monroe *et al.*, *PRX Quantum* **2**, 017003 (2021).
- [5] I. Bloch, J. Dalibard, and S. Nascimbene, *Nat. Phys.* **8**, 267 (2012).

- [6] H. Bernien, S. Schwartz, A. Keesling, H. Levine, A. Omran, H. Pichler, S. Choi, A. S. Zibrov, M. Endres, M. Greiner, V. Vuletić, and M. D. Lukin, *Nature (London)* **551**, 579 (2017).
- [7] U. Bissbort, D. Cocks, A. Negretti, Z. Idziaszek, T. Calarco, F. Schmidt-Kaler, W. Hofstetter, and R. Gerritsma, *Phys. Rev. Lett.* **111**, 080501 (2013).
- [8] A. Alexandrov and J. Ranninger, *Phys. Rev. B* **24**, 1164 (1981).
- [9] A. Lanzara, P. Bogdanov, X. Zhou, S. Kellar, D. Feng, E. Lu, T. Yoshida, H. Eisaki, A. Fujimori, K. Kishio *et al.*, *Nature (London)* **412**, 510 (2001).



- [10] G. Pupillo, A. Griessner, A. Micheli, M. Ortner, D.-W. Wang, and P. Zoller, *Phys. Rev. Lett.* **100**, 050402 (2008).
- [11] M. Ortner, A. Micheli, G. Pupillo, and P. Zoller, *New J. Phys.* **11**, 055045 (2009).
- [12] J. Hague and C. MacCormick, *New J. Phys.* **14**, 033019 (2012).
- [13] K. Jachymski and A. Negretti, *Phys. Rev. Res.* **2**, 033326 (2020).
- [14] J. T. Wilson, S. Saskin, Y. Meng, S. Ma, R. Dilip, A. P. Burgers, and J. D. Thompson, *Phys. Rev. Lett.* **128**, 033201 (2022).
- [15] Y. Mei, Y. Li, H. Nguyen, P. R. Berman, and A. Kuzmich, *Phys. Rev. Lett.* **128**, 123601 (2022).
- [16] I. Lang and Y. A. Firsov, *Sov. Phys. JETP* **16**, 1301 (1963).
- [17] G. Wellein, H. Röder, and H. Fehske, *Phys. Rev. B* **53**, 9666 (1996).
- [18] Y. Takada and A. Chatterjee, *Phys. Rev. B* **67**, 081102(R) (2003).
- [19] R. T. Clay and R. P. Hardikar, *Phys. Rev. Lett.* **95**, 096401 (2005).
- [20] M. Hohenadler and W. von der Linden, in *Polarons in Advanced Materials* (Springer, New York, 2007), pp. 463–502.
- [21] K.-M. Tam, S.-W. Tsai, and D. K. Campbell, *Phys. Rev. B* **89**, 014513 (2014).
- [22] T. Yin, D. Cocks, and W. Hofstetter, *Phys. Rev. A* **92**, 063635 (2015).
- [23] Y. Wang, I. Esterlis, T. Shi, J. I. Cirac, and E. Demler, *Phys. Rev. Res.* **2**, 043258 (2020).
- [24] S. de Léséleuc, V. Lienhard, P. Scholl, D. Barredo, S. Weber, N. Lang, H. P. Büchler, T. Lahaye, and A. Browaeys, *Science* **365**, 775 (2019).
- [25] P. Sompet, S. Hirthe, D. Bourgund, T. Chalopin, J. Bibo, J. Koepsell, P. Bojović, R. Verresen, F. Pollmann, G. Salomon *et al.*, *Nature (London)* **606**, 484 (2022).
- [26] S. Weber, C. Tresp, H. Menke, A. Urvoy, O. Firstenberg, H. P. Büchler, and S. Hofferberth, *J. Phys. B: At., Mol. Opt. Phys.* **50**, 133001 (2017).
- [27] G. D. Mahan, *Many-Particle Physics* (Springer, New York, 2013).
- [28] U. Bissbort, W. Hofstetter, and D. Poletti, *Phys. Rev. B* **94**, 214305 (2016).
- [29] F. M. Gambetta, W. Li, F. Schmidt-Kaler, and I. Lesanovsky, *Phys. Rev. Lett.* **124**, 043402 (2020).
- [30] S. Whitlock, A. W. Glaetzle, and P. Hannaford, *J. Phys. B: At., Mol. Opt. Phys.* **50**, 074001 (2017).
- [31] N. Marzari and D. Vanderbilt, *Phys. Rev. B* **56**, 12847 (1997).
- [32] W. Ganczarek, M. Modugno, G. Pettini, and J. Zakrzewski, *Phys. Rev. A* **90**, 033621 (2014).
- [33] A. Negretti, R. Gerritsma, Z. Idziaszek, F. Schmidt-Kaler, and T. Calarco, *Phys. Rev. B* **90**, 155426 (2014).
- [34] T. Gould and T. Bucko, *J. Chem. Theory Comput.* **12**, 3603 (2016).
- [35] C. S. Adams, J. D. Pritchard, and J. P. Shaffer, *J. Phys. B: At., Mol. Opt. Phys.* **53**, 012002 (2019).
- [36] C. Chin, R. Grimm, P. Julienne, and E. Tiesinga, *Rev. Mod. Phys.* **82**, 1225 (2010).
- [37] M. Mueller, R. S. Said, F. Jelezko, T. Calarco, and S. Montangero, *Rep. Prog. Phys.* **85**, 076001 (2022).
- [38] F. Mazzoncini, V. Cavina, G. M. Andolina, P. A. Erdman, and V. Giovannetti, *arXiv:2210.04028*.
- [39] D. Barredo, V. Lienhard, P. Scholl, S. de Léséleuc, T. Boulier, A. Browaeys, and T. Lahaye, *Phys. Rev. Lett.* **124**, 023201 (2020).
- [40] C. Kokail, C. Maier, R. van Bijnen, T. Brydges, M. K. Joshi, P. Jurcevic, C. A. Muschik, P. Silvi, R. Blatt, C. F. Roos *et al.*, *Nature (London)* **569**, 355 (2019).
- [41] M. Meth, V. Kuzmin, R. van Bijnen, L. Postler, R. Stricker, R. Blatt, M. Ringbauer, T. Monz, P. Silvi, and P. Schindler, *Phys. Rev. X* **12**, 041035 (2022).
- [42] T. Shi and J. I. Cirac, *Phys. Rev. A* **87**, 013606 (2013).
- [43] I. Reshodko, A. Benseny, J. Romhányi, and T. Busch, *New J. Phys.* **21**, 013010 (2019).
- [44] T. Salamon, A. Celi, R. W. Chhajlany, I. Frérot, M. Lewenstein, L. Tarruell, and D. Rakshit, *Phys. Rev. Lett.* **125**, 030504 (2020).
- [45] J. Knörzner, T. Shi, E. Demler, and J. I. Cirac, *Phys. Rev. Lett.* **128**, 120404 (2022).
- [46] M. Di Liberto, A. Kruckenhauser, P. Zoller, and M. A. Baranov, *Quantum* **6**, 731 (2022).
- [47] A. Cavigliari, *Contemp. Phys.* **59**, 31 (2018).
- [48] M. Babadi, M. Knap, I. Martin, G. Refael, and E. Demler, *Phys. Rev. B* **96**, 014512 (2017).
- [49] A. L. Fetter and J. D. Walecka, *Quantum Theory of Many-Particle Systems* (Courier, New York, 2012).